

Communication

MoSe₂ with Ultra-Fine Pt Decoration for Efficient Photodegradation

Yong Chen ¹, Dawei Shao ¹, Fupeng Xu ¹, Zhongjia Huang ² and Xinying Shi ^{1,*} ¹ School of Physics and Electronic Engineering, Jiangsu Normal University, Xuzhou 221116, China² Anhui Key Laboratory of High-Performance Non-Ferrous Metal Materials, Anhui Polytechnic University, Wuhu 241000, China

* Correspondence: xshi@jsnu.edu.cn

Abstract: Transition metal dichalcogenides are widely studied for their photocatalytic ability due to the adjustable bandgap, high carrier mobility and possibility of foreign-element doping. In this work, multilayer molybdenum diselenide (MoSe₂) was decorated with ultra-fine Pt nanoparticles through the mild hydrothermal method. MoSe₂-Pt nanocomposites were synthesized and showed good structural and chemical stabilities. The incorporation of Pt nanoparticles provides plenty of active sites for MoSe₂. The dominant Pt particle sizes are 1.8 nm, 1.8 nm, and 1.9 nm for the three synthesized samples, respectively. The mean crystal sizes of Pt (111) were calculated from X-ray diffraction patterns and we found that they were in accordance with the particle sizes. Both the particle sizes and mean crystal sizes are related to the synthesis conditions. X-ray photoelectron spectroscopy (XPS) characterizations revealed the formation of Se–Pt bonding. The relative contents of Pt–Se bonding were also calculated from XPS results, and they show the same trends as the optical absorption properties. Combining the XPS and optical absorption results, the effects of Se–Pt bonding during the photo-related process could be further confirmed. By degrading methylene blue (MB) under visible light, the synthesized nanocomposites proved promising for application in real-case degradation of organic pollutants. The sample synthesized with a moderate content of MoSe₂ exhibited the best photodegradation efficiency, which could be explained by the maximum Pt–Se contents. Based on the experimental findings, we proposed a possible photodegradation mechanism.

Keywords: MoSe₂; photodegradation; photocatalyst; two-dimensional materials

Citation: Chen, Y.; Shao, D.; Xu, F.; Huang, Z.; Shi, X. MoSe₂ with Ultra-Fine Pt Decoration for Efficient Photodegradation. *Appl. Sci.* **2024**, *14*, 3592. <https://doi.org/10.3390/app14093592>

Academic Editors: Robert A. Varin and Geng Zhong

Received: 17 March 2024

Revised: 20 April 2024

Accepted: 21 April 2024

Published: 24 April 2024



Copyright: © 2024 by the authors. Licensee MDPI, Basel, Switzerland. This article is an open access article distributed under the terms and conditions of the Creative Commons Attribution (CC BY) license (<https://creativecommons.org/licenses/by/4.0/>).

1. Introduction

Photodegradation of organic pollutants in natural water has been studied for several decades [1,2]. By employing sunlight and semiconducting materials, redox reactions could be taking place to degrade and remove those dissolved pollutants, especially organic dyes [3] such as methylene blue, methyl orange, bisphenol A (BPA), etc. It provides a green and sustainable route for natural water purification. Among so many semiconducting candidates, transition metal dichalcogenides (TMDs) are known for their suitable bandgaps for visible light absorption and utilization [4,5]. As layered two-dimensional materials, TMDs are formed by covalence bonds in layers and van der Waals forces between layers [6]. Such a layered structure also brings an adjustable bandgap which can be easily manipulated by controlling the layer numbers [7]. They usually have active edge sites due to various types of defects but a relatively inert basal surface [8,9]. Thanks to their host ability for incorporating dopants, especially noble metal nanoparticles, the light–matter interaction as well as the photocatalytic performance could be improved. In this case, members of the TMD group are currently featured as photocatalysts for hydrogen evolution and organic-pollutant decomposition in water [10]. It is believed that the TMDs would hopefully provide a solution towards current fossil fuel deficiency and natural water pollution problems.

As a typical member of the TMD family, molybdenum diselenide (MoSe₂) has similar atomic arrangements to molybdenum disulfide (MoS₂) [11], and has been widely

investigated for applications such as transistors, gas sensors, photodetectors and photocatalysts [12,13]. For example, n-MoSe₂ transistors perform well in detecting the streptavidin molecule, due to the controllable high reverse current [14]. As for photocatalytic ability, researchers proposed the hydrothermal synthesis method to prepare MoSe₂ for hydrogen evolution reactions and organic dye degradations [15]. MoSe₂ is stacked into layers of Se-Mo-Se sandwich planes through the van der Waals force. The typically tunable bandgap also exists in MoSe₂, making it suitable for light absorption among a wide range of wavelengths. It should be mentioned that MoSe₂ has relatively smaller band gap than MoS₂, which brings more efficient photoexcitation [16]. In the photocatalytic applications, researchers proposed several routes to improve its total activities. For instance, the typical core-shell structures are beneficial for strong chemical activities which could be achieved by incorporating carbon nanotubes, MoS₂ nanoflakes, and transition metals, especially noble metals [17–21]. The optical absorption of MoSe₂ has been successfully adjusted by phase engineering, providing another choice for obtaining efficient photocatalytic performance [22]. Moreover, it is also possible to form Z-scheme nanocomposites by introducing other semiconducting materials [23,24]. Among the above methods, noble-metal doping is an effective and controllable way. Noble metal nanoparticles could be easily anchored to MoSe₂ edges due to the commonly existing Se defects. However, it usually requires sophisticated synthesis to activate the inert MoSe₂ basal planes [8]. For instance, there should be a pre-synthesis to prepare MoSe₂@mesoporous hollow carbon spheres, and the following step to obtain the incorporation of Pt nanoparticles [25].

Herein, we report a feasible and straightforward synthetic method to introduce Pt nanoparticles onto MoSe₂. The Pt nanoparticles are well formed and their sizes are controlled within 2.3 nm, which could be called ultra-fine Pt nanoparticles. The synthesized MoSe₂-Pt nanocomposites exhibit great structural and chemical stabilities. The introduced Pt nanoparticles provide plenty of active sites for light absorption and photocatalysis. We performed the photodegradation of MB under visible light irradiation. It has been found that the synthesized materials could decompose MB efficiently compared to pristine MoSe₂. Such improved photocatalytic performance has been explained by the enhanced light absorption and photoelectron transportation. Using X-ray photoelectron spectroscopy (XPS), the chemical bonding between Se and Pt was confirmed. It explains not only the great stabilities of the compounds but also the efficient channels for charge transfer during photocatalytic reactions. The Pt–Se bonding also contributes to the enhanced visible light absorption. Considering the excellent photocatalytic properties of the MoSe₂-Pt nanocompounds, we believe that the reported synthetic method might be suitable for further investigation and mass production.

2. Materials and Methods

2.1. Materials and Sample Preparations

The materials were purchased from Sigma-Aldrich (St. Louis, MA, USA) with analytical grade, and deionized water was produced at our own lab. The MoSe₂-Pt samples were synthesized with the following steps: (a) multilayer MoSe₂ nanopowders were dispersed into deionized water with various ratios. The concentration of MoSe₂ suspension was 0.1 mg/mL, 0.2 mg/mL and 0.3 mg/mL, respectively. (b) In order to obtain Pt nanoparticles with an extremely small size, K₂PtCl₄ and trisodium citrate were used as precursors to obtain Pt nanoparticles [26,27]. K₂PtCl₄ and trisodium citrate were added into the MoSe₂ suspension by mechanically stirring. (3) The mixed solution was set under an ultrasonic bath at 50 °C for 150 min or 200 min. (4) Pt⁰ can be reduced from PtCl₄²⁻, and Pt nanoparticles would finally grow onto MoSe₂ nanoflakes. After synthesis, three samples with different mass ratios were obtained, as shown in Table 1. These samples are labelled according to their contents, which were M1Pt, M2Pt and M3Pt, respectively.

Table 1. The synthetic details of the samples.

Samples	MoSe ₂	K ₂ PtCl ₄	Conditions
M1Pt	0.1 mg/mL × 10 mL	41.5 mg	50 °C, 150 min
M2Pt	0.2 mg/mL × 10 mL	41.5 mg	50 °C, 150 min
M3Pt	0.3 mg/mL × 10 mL	41.5 mg	50 °C, 200 min

2.2. Characterizations

The sample morphologies were studied through a transmission electron microscope (TEM, JEOL 2200FS (JEOL, Tokyo, Japan)). The crystal structures of MoSe₂ and the synthesized complexes were measured through X-ray diffraction (XRD, Bruker (Billerica, MA, USA)). Cu K α emission ($\lambda = 1.5406 \text{ \AA}$) was employed as the X-ray source. The optical properties were measured through a Lambda 950 UV-Vis spectrophotometer (Spectralab Scientific Inc., Markham, ON, Canada) with BaSO₄ as reference. The synthesized powder was dissolved in deionized water for UV-vis absorption tests. The chemical states were analyzed by Thermo Fisher (Waltham, MA, USA) K-Alpha X-ray photoelectron spectroscopy.

2.3. Photodegradation Measurements

The photocatalytic properties of the synthesized MoSe₂-Pt catalysts were studied by degrading Methylene blue (MB). During each photocatalytic reaction, 50 mg of the catalyst was put in 50 mL of MB solution (10 mg/L). Reactions were carried out under a 300 W Xe lamp. We used a cutoff filter (#84-689, TECHSPEC, Co., Ltd., Gauteng, South Africa) to block the light under the wavelength of 400 nm. Before degradation tests, MB solutions with catalysts inside were stirred under a dark environment for half an hour to dispose of the adsorption/desorption effects. During photocatalytic degradations, 2 mL of the solution was taken every 30 min and was centrifuged to remove the MoSe₂-Pt powder. Visible-light absorption spectra ranging from 400 nm to 800 nm were measured through a Lambda 950 UV-Vis spectrophotometer. During measurements, the absorption peak of MB was set at 664 nm and the concentration of residual MB could be determined by the integration of the MB absorption peaks. The photocatalytic reactions were therefore presented by time-course decrease in MB concentration.

3. Results and Discussion

3.1. MoSe₂-Pt Morphologies and Crystal Structures

After synthesis, a drop of the solution containing MoSe₂-Pt was placed onto a holey carbon grid and dried in air. Then the samples were observed under TEM. The morphologies of MoSe₂ flakes among the three samples were similar in shape and size. Therefore, we chose sample M1Pt as an example whose morphologies are shown in Figure 1. In Figure 1a, MoSe₂ nanoflakes are of a round shape with a typical size of 40 nm. There are tiny Pt dots on the edge of the MoSe₂. The Pt dots are clearer in the zoomed-in image in Figure 1b. Due to the mild synthetic conditions and low concentration of K₂PtCl₄ in solution 1, PtCl₄²⁻ was reduced to ultrafine particles. There are more Pt nanoparticles formed on the edge sites compared to the surfaces of the MoSe₂ because the edge sites are more reactive than the basal planes [28]. Although very small in size, the Pt particles were well crystallized in (111) phase with a lattice spacing of 2.29 Å, as shown in Figure 1c. Such crystalline structure is compatible with the MoSe₂ (100) facet. It suggests the Pt particles are well grown on MoSe₂. Figure 1d–f show the distribution of Pt nanoparticles for the samples of M1Pt, M2Pt, and M3Pt, respectively. It can be seen that the samples of M1Pt and M2Pt have the same dominant Pt size of 1.8 nm, while M3Pt has a slightly larger Pt size of 1.9 nm.

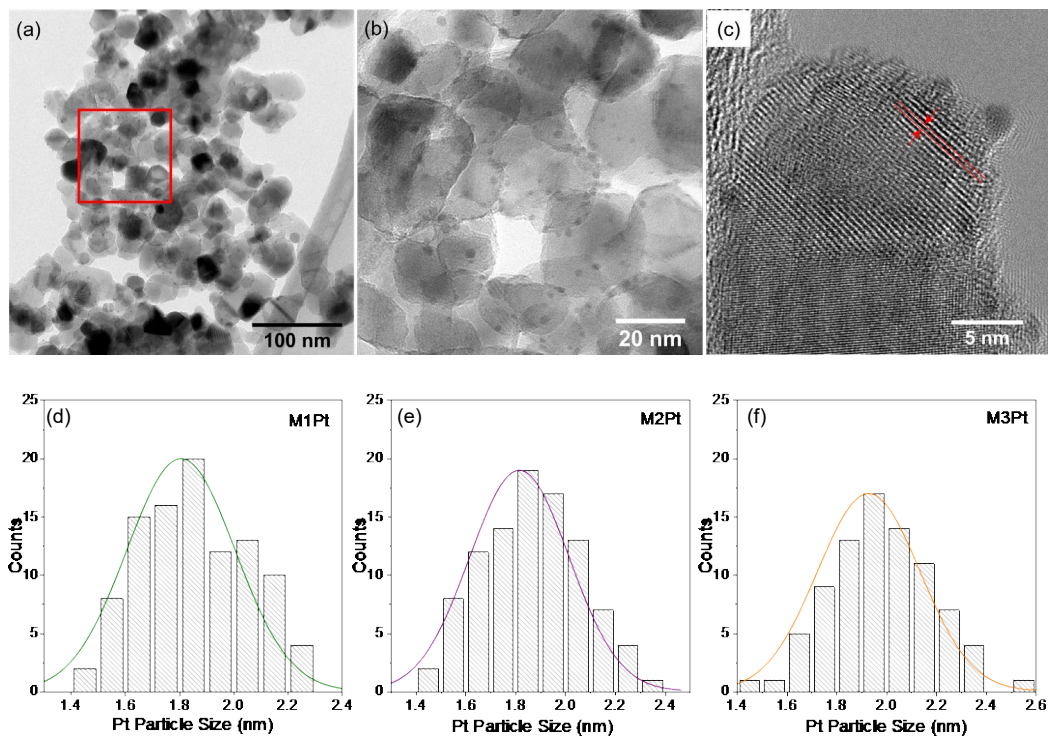


Figure 1. Morphologies of MoSe₂-Pt samples. (a) TEM image of MoSe₂-Pt; (b) zoomed-in image of the squared region in (a); (c) HR-TEM image shows the crystal structure of Pt; (d–f) Pt size distributions of the samples of M1Pt, M2Pt, and M3Pt, respectively.

In Figure 2, the XRD spectra show the crystal structure of the three samples of MoSe₂-Pt nanocomposites and pristine MoSe₂ nanopowder. The crystal planes of MoSe₂ and Pt were marked with diamonds and stars, respectively. The MoSe₂ (100), (103), (105), (110) and (200) planes were identified from both samples, which was in good agreement with previous reports [29]. Compared to the pristine MoSe₂, Figure 2 shows that MoSe₂ is stable and keeps its crystal structure after synthesis.

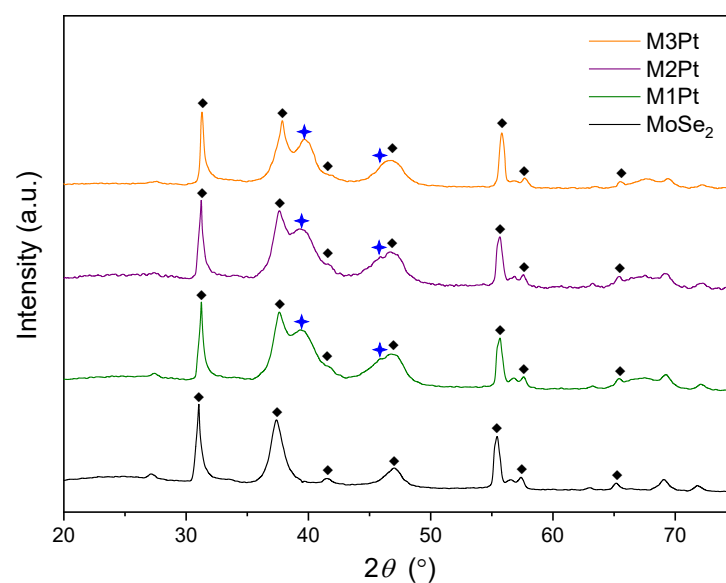


Figure 2. XRD spectra of the synthesized MoSe₂-Pt nanocomposite and MoSe₂ nanopowder.

Pt (111) and (200) planes were identified in the synthesized MoSe₂-Pt samples. The Pt (111) lattice spacings are shown in Table 2. We can see that Pt (111) peak positions were slightly varied among the three samples. The lattice spacings are calculated as 0.2285, 0.2291, and 0.2274 nm, respectively. Moreover, the mean crystal sizes (D (111) in Table 2) were also calculated through Scherrer's equation [30]. They are very close for the M1Pt and M2Pt samples, while slightly larger for the M3Pt sample. It should be noted that the calculated mean crystal sizes are not the particle sizes which could be directly measured under TEM; however, the D (111) values show the same trends with the particle sizes shown in Figure 1d–f.

Table 2. Pt (111) lattice spacings and mean crystal sizes.

Samples	$2\theta/^\circ$	FWHM/ $^\circ$	d (111)/nm	D (111)/nm
M1Pt	39.40	12.4217	0.2285	0.6793
M2Pt	39.30	12.4017	0.2291	0.6802
M3Pt	39.60	12.0752	0.2274	0.6992

3.2. Chemical States, Mechanism of Efficient Photocatalytic Reactions

The chemical electronic states of the MoSe₂-Pt samples were evaluated through XPS. The high-resolution XPS spectra of Pt 4f and Se 3d are shown in Figure 3. In Figure 3a–c, there are two Pt species which were identified by fitting the original Pt 4f spectra. Pt⁰ peaks are the reduced Pt nanoparticles in metal form, and Pt–Se peaks are attributed to the Pt–Se bonding. The binding energies of these Pt peaks are slightly shifted among the three samples which may be caused by partial electron transfer between MoSe₂ and Pt [31]. In Figure 3d–f, two main contents are found in the Se 3d spectra, which are the Se–Mo peaks and Se–Pt peaks. Such results are typical for MoSe₂ and PtSe₂ characteristics [32], and further confirm the formation of Se–Pt bonding. Therefore, it is obvious that chemical bonding of Pt–Se formed after the synthesis. Such chemical bonding can provide an effective pathway for charge transportation during photocatalytic reactions [9]. The Se–Mo 3d_{5/2} peaks at 54.56 eV are barely shifted among the three samples, suggesting that MoSe₂ takes a dominant content compared to the Se–Pt species.

Based on the XPS results, it is noticed that the relative contents of Pt–Se varies among the samples, which may have influence on electron transportation. The relative contents of Pt–Se can be calculated from Pt 4f spectra, which are 34.78%, 40.02%, and 19.79%, respectively. It suggests that too much MoSe₂ involved in the synthesis (the M3Pt sample) may limit the formation of Pt–Se bonding.

In this case, there may be two ways that the photocatalytic abilities could be affected. Firstly, Pt–Se bonding provides an efficient pathway for charge transfer, so more contents of Pt–Se would be beneficial to the photocatalytic reactions. Secondly, the existence of Pt nanoparticles (Pt⁰) can be confirmed by TEM results in Figure 1. Such ultra-fine Pt nanoparticles offer active sites for photocatalytic reactions where degradation could take place [33]. Introducing noble metal nanoparticles on edge sites of MoSe₂ is a typical method for enhancing the photocatalytic properties.

3.3. Optical Properties of the Catalysts

In order to evaluate the optical performance of the synthesized samples, they were prepared in aqua solution for UV–visible absorption measurements. Figure 4 shows the absorption spectra of MoSe₂ and the three samples. In the visible wavelength range, there are obvious absorption peaks at around 475 nm and 710 nm, respectively. Such optical behavior is typical for multilayer MoSe₂ on a nanometer scale [34]. It can be seen that the pristine MoSe₂ has a weak response to visible light, while the MoSe₂-Pt samples strongly absorb the short wavelength of visible light, mainly between 450 and 550 nm. Among the three synthesized samples, M2Pt shows the best absorption ability for visible light while M3Pt shows the worst. Moreover, there is slight red-shift between the pristine MoSe₂ and

the catalysts. Such feature enhances the absorption of light in a longer wavelength, making it suitable for the utilization of the solar spectrum.

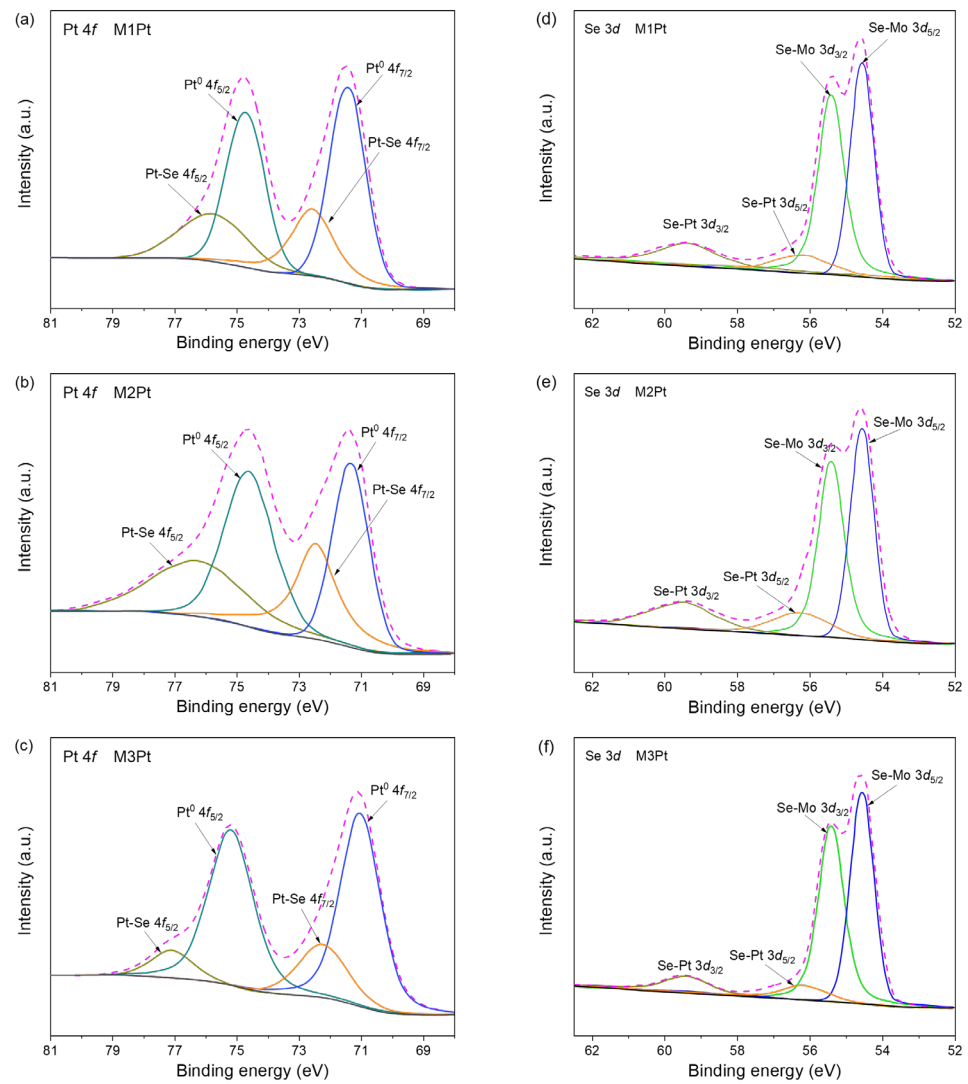


Figure 3. XPS spectra of the synthesized MoSe₂-Pt samples. (a) Pt 4f of M1Pt, (b) Pt 4f of M2Pt, (c) Pt 4f of M3Pt, (d) Se 3d of M1Pt, (e) Se 3d of M2Pt, (f) Se 3d of M3Pt.

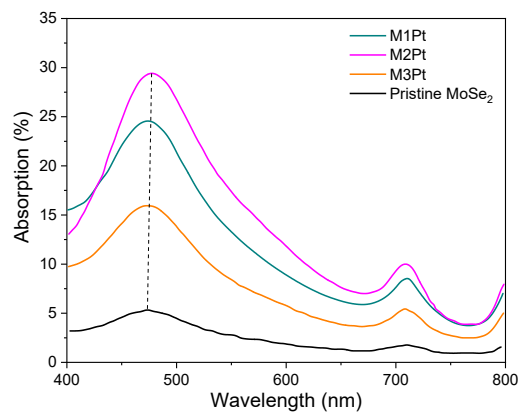


Figure 4. UV-vis absorption spectra of MoSe₂ and the synthesized samples.

3.4. Photodegradation

The aforementioned characterizations provide chemical and optical insights into the synthesized materials. Their photocatalytic performance is evaluated by MB degradation, as shown in Figure 5. The time-course photodegradation results are shown in Figure 5a. Here, C/C_0 is used to represent the decrease of MB concentration, where C_0 and C are the original MB concentration and the MB concentration at a certain time, respectively. The dark process suggests that the synthesized materials show obvious adsorption of MB, while the pristine MoSe_2 can hardly adsorb MB. Such adsorption abilities are usually related to the photocatalytic process. We can see that pristine MoSe_2 can hardly degrade MB and the samples are all reactive with MB. Within around 60 min, MB is nearly removed by the samples of M1Pt and M2Pt. However, the M3Pt sample performs slightly less efficiently, but it can still degrade more than 90% of MB after 120 min. Such photocatalytic results are in accordance with the optical absorption properties shown in Figure 4. Considering the catalyst amount used in the degradation process, the above photocatalytic performance is comparable to other popular photocatalysts, such as $\text{Bi}_2\text{WO}_6/\text{BiOCl}$ [35]. As a comparison, pristine MoSe_2 removes only 5.4% of the MB in 120 min with the same irradiation condition. It suggests that the introduction of Pt to MoSe_2 edges greatly improves the photocatalytic property.

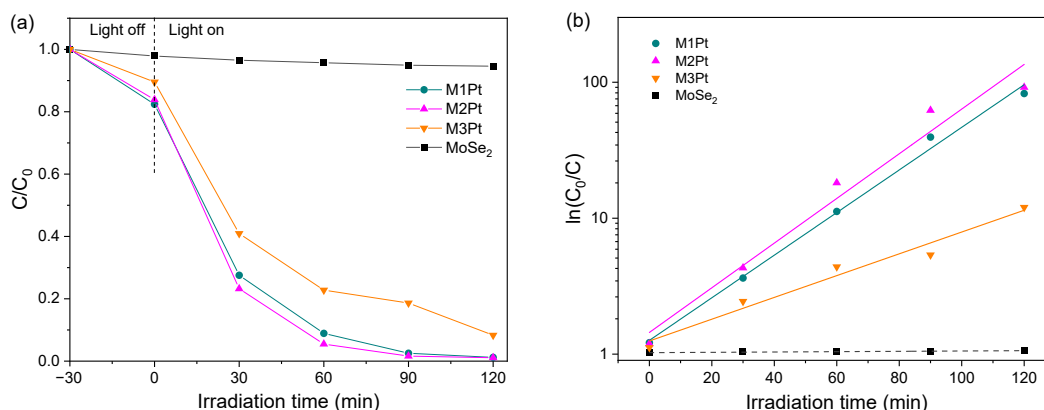


Figure 5. The time-course photocatalytic MB degradation under visible light irradiation. (a) Photodegradation of the synthesized samples and pristine MoSe_2 . (b) Photodegradation kinetics of $\ln(C_0/C)$.

The photodegradation kinetics was evaluated by the pseudo-first-order model. With this model, the pseudo-first-order constant k could be expressed as

$$k = \frac{\ln(C_0/C)}{t} \quad (1)$$

The results of $\ln(C_0/C)$ are shown in Figure 5b. The constants were calculated as 0.0361 min^{-1} , 0.0379 min^{-1} , and 0.0185 min^{-1} for the three samples, respectively. It is obvious that the M2Pt sample has the best photocatalytic kinetics. The constant values have the same trends as the Pt–Se contents. This indicates the correlation between Se–Pt bonding and photocatalytic performance. On the other hand, k values are not linearly affected by either the Pt amount used in the synthesis nor the relative contents of Pt–Se bonding. This may indicate that the surface segregation occurred during synthesis [36].

The possible photocatalytic mechanism can therefore be discussed. During the degradation process, photo-generated electrons from valence bands of MoSe_2 reach the conduction bands, and finally migrate to the active sites provided by Pt nanoparticles. The electron-hole pairs participate in redox reactions, where the holes oxidize water to H^+ and $\cdot\text{OH}$. The hydroxyl radicals then react with MB [9]. Meanwhile, the electrons reduce H^+

to ·H. The Pt–Se bonding offers stable and efficient routes for charge transfer during the whole process.

4. Conclusions

In conclusion, we synthesized MoSe₂-Pt complexes with a facile method, where Pt is reduced to ultra-fine nanoparticles. The synthetic method is simple and straightforward, making it suitable for mass production. The synthesized samples show a greatly enhanced photocatalytic performance for degrading the organic pollutant of MB under visible-light irradiation. Such properties show the excellent ability of visible-light utilization. The photodegradation mechanism could be explained through XPS analysis. Effective Pt–Se bonding provides pathways for charge transportation and ultra-fine Pt nanoparticles offer active sites for photocatalytic reactions. This work may be helpful for further photocatalyst design and applications in real cases.

Author Contributions: Y.C., investigation, characterization, and writing—original draft; D.S., characterization; F.X., characterization; Z.H., investigation, revision; X.S., supervision and writing—review and editing. All authors have read and agreed to the published version of the manuscript.

Funding: This work was financially supported by the Natural Science Foundation of Jiangsu Higher Education Institutions of China (No. 19KJB140008), and the Anhui Provincial Natural Science Foundation (No. 2008085ME141).

Institutional Review Board Statement: Not applicable.

Informed Consent Statement: Not applicable.

Data Availability Statement: The original contributions presented in the study are included in the article, further inquiries can be directed to the corresponding author.

Conflicts of Interest: The authors declare no conflicts of interest.

References

1. Sellers, P.; Kelly, C.A.; Rudd, J.W.M.; MacHutchon, A.R. Photodegradation of methylmercury in lakes. *Nature* **1996**, *380*, 694–697. [[CrossRef](#)]
2. Saeed, M.; Muneer, M.; Haq, A.U.; Akram, N. Photocatalysis: An effective tool for photodegradation of dyes—A review. *Environ. Sci. Pollut. Res.* **2022**, *29*, 293–311. [[CrossRef](#)] [[PubMed](#)]
3. Jiang, Q.; Lu, Y.; Huang, Z.; Hu, J. Facile solvent-thermal synthesis of ultrathin MoSe₂ nanosheets for hydrogen evolution and organic dyes adsorption. *Appl. Surf. Sci.* **2017**, *402*, 277–285. [[CrossRef](#)]
4. Chen, C.; Ma, W.; Zhao, J. Semiconductor-mediated photodegradation of pollutants under visible-light irradiation. *Chem. Soc. Rev.* **2010**, *39*, 4206–4219. [[CrossRef](#)] [[PubMed](#)]
5. Krasnok, A.; Lepeshov, S.; Alú, A. Nanophotonics with 2D transition metal dichalcogenides. *Opt. Express* **2018**, *26*, 15972. [[CrossRef](#)]
6. Chhowalla, M.; Liu, Z.; Zhang, H. Two-dimensional transition metal dichalcogenide (TMD) nanosheets. *Chem. Soc. Rev.* **2015**, *44*, 2584. [[CrossRef](#)]
7. Tan, C.; Zhang, H. Two-dimensional transition metal dichalcogenide nanosheet-based composites. *Chem. Soc. Rev.* **2015**, *44*, 2713. [[CrossRef](#)]
8. Kibsgaard, J.; Chen, Z.; Reinecke, B.N.; Jaramillo, T.F. Engineering the surface structure of MoS₂ to preferentially expose active edge sites for electrocatalysis. *Nat. Mater.* **2012**, *11*, 963–969. [[CrossRef](#)]
9. Shi, X.; Posyasaev, S.; Huttula, M.; Pankratov, V.; Hoszowska, J.; Dousse, J.C.; Zeeshan, F.; Niu, Y.; Zakharov, A.; Li, T.; et al. Metallic contact between MoS₂ and Ni via Au nanoglue. *Small* **2018**, *14*, 1704526. [[CrossRef](#)]
10. Shi, X.; Zhang, M.; Wang, X.; Kistanov, A.A.; Li, T.; Cao, W.; Huttula, M. Nickel nanoparticle-activated MoS₂ for efficient visible light photocatalytic hydrogen evolution. *Nanoscale* **2022**, *14*, 8601–8610. [[CrossRef](#)]
11. Shim, G.W.; Yoo, K.; Seo, S.B.; Shin, J.; Jung, D.Y.; Kang, I.S.; Ahn, C.W.; Cho, B.J.; Choi, S.Y. Large-area single-layer MoSe₂ and its van der Waals heterostructures. *ACS Nano* **2014**, *8*, 6655–6662. [[PubMed](#)]
12. Mathew, S.; Sai Chandu, K.K.; Halder, S.; Polumati, G.; Chakraborty, C.; Sahatiya, P.; Pal, S. Band alignment and charge transport study of Au nanoparticles decorated over MoS₂/MoSe₂ hybrid heterostructure for plasmon enhanced photodetection. *Mater. Sci. Semicond. Process.* **2023**, *156*, 107302. [[CrossRef](#)]
13. Kumar, S.; Mirzaei, A.; Kumar, A.; Lee, M.H.; Ghahremani, Z.; Kim, T.U.; Kim, J.Y.; Kwoka, M.; Kumar, M.; Kim, S.S.; et al. Nanoparticles anchored strategy to develop 2D MoS₂ and MoSe₂ based room temperature chemiresistive gas sensors. *Coord. Chem. Rev.* **2024**, *503*, 215657. [[CrossRef](#)]

14. Nisar, S.; Dastgeer, G.; Shahzadi, M.; Shahzad, Z.M.; Elahi, E.; Irfan, A.; Eom, J.; Kim, H.; Kim, D.K. Gate-assisted MoSe₂ transistor to detect the streptavidin via supporter molecule engineering. *Mater. Today Nano* **2023**, *24*, 100405. [[CrossRef](#)]
15. Shi, H.; Zhang, H.; Li, M.; Wang, Y.; Wang, D. Nanoflower-like 1T/2H mixed-phase MoSe₂ as an efficient electrocatalyst for hydrogen evolution. *J. Alloys Compd.* **2021**, *878*, 160381. [[CrossRef](#)]
16. Zhang, Y.; Chang, T.R.; Zhou, B.; Cui, Y.T.; Yan, H.; Liu, Z.; Schmitt, F.; Lee, J.; Moore, R.; Chen, Y.; et al. Direct observation of the transition from indirect to direct bandgap in atomically thin epitaxial MoSe₂. *Nat. Nanotech.* **2014**, *9*, 111–115. [[CrossRef](#)] [[PubMed](#)]
17. Maity, S.; Das, B.; Samanta, M.; Das, B.K.; Ghosh, S.; Chattopadhyay, K.K. MoSe₂-Amorphous CNT Hierarchical Hybrid Core-Shell Structure for Efficient Hydrogen Evolution Reaction. *ACS Appl. Energy Mater.* **2020**, *3*, 5067–5076. [[CrossRef](#)]
18. Hwang, Y.; Shin, N. Colloidal Synthesis of MoSe₂/WSe₂ Heterostructure Nanoflowers via Two-Step Growth. *Materials* **2021**, *14*, 7294. [[CrossRef](#)] [[PubMed](#)]
19. Su, J.; Nie, Z.; Feng, Y.; Hu, X.; Li, H.; Zhao, Z.; Zan, S.; Qi, S. Hollow core-shell structure Co/C@MoSe₂ composites for high-performance microwave absorption. *Compos. Part A Appl. Sci. Manuf.* **2022**, *162*, 107140. [[CrossRef](#)]
20. Rao, B.G.; Matte, H.S.S.R.; Rao, C.N.R. Decoration of few-layer graphene-like MoS₂ and MoSe₂ by noble metal nanoparticles. *J. Clust. Sci.* **2012**, *23*, 929–937.
21. Upadhyay, S.N.; Pakhira, S. Nanostructured Pt-doped 2D MoSe₂: An efficient bifunctional electrocatalyst for both hydrogen evolution and oxygen reduction reactions. *Phys. Chem. Chem. Phys.* **2022**, *37*, 22823–22844. [[CrossRef](#)] [[PubMed](#)]
22. Hanson, E.D.; Lilley, L.M.; Cain, J.D.; Hao, S.; Palacios, E.; Aydin, K.; Wolverson, C.; Meade, T.; Dravid, V.P. Phase engineering and optical properties of 2D MoSe₂: Promise and pitfalls. *Mater. Chem. Phys.* **2019**, *225*, 219–226. [[CrossRef](#)]
23. Wang, F.; Lu, T.; Cheng, X.; Zhang, Y.; Xiao, X. Fabrication of MoSe₂/Bi₃O₄Br Z-scheme heterojunction with enhanced photocatalytic performance. *J. Environ. Chem. Eng.* **2024**, *12*, 111991. [[CrossRef](#)]
24. Wang, X.; Wang, X.; Huang, J.; Li, S.; Meng, A.; Li, Z. Interfacial chemical bond and internal electric field modulated Z-scheme S_v-ZnIn₂S₄/MoSe₂ photocatalyst for efficient hydrogen evolution. *Nat. Commun.* **2021**, *12*, 4112. [[CrossRef](#)] [[PubMed](#)]
25. Yang, F.; Qiao, W.; Yu, L.; Wang, S.; Feng, L. Support engineering modulated Pt/hierarchical MoSe₂@mesoporous hollow carbon spheres for efficient methanol-assisted water splitting. *Chem. Eng. J.* **2024**, *483*, 149055. [[CrossRef](#)]
26. Huang, X.; Zeng, Z.; Bao, S.; Wang, M.; Qi, X.; Fan, Z.; Zhang, H. Solution-phase epitaxial growth of noble metal nanostructures on dispersible single-layer molybdenum disulfide nanosheets. *Nat. Commun.* **2013**, *4*, 1444. [[CrossRef](#)]
27. Lin, C.S.; Khan, M.R.; Lin, S.D. Platinum states in citrate sols by EXAFS. *J. Colloid Interface Sci.* **2005**, *287*, 366–369. [[CrossRef](#)] [[PubMed](#)]
28. Tsai, C.; Chan, K.; Abild-Pedersen, F.; Nørskov, J.K. Active edge sites in MoSe₂ and WSe₂ catalysts for the hydrogen evolution reaction: A density functional study. *Phys. Chem. Chem. Phys.* **2014**, *16*, 13156–13164. [[CrossRef](#)]
29. Shelke, N.T.; Late, D.J. Hydrothermal growth of MoSe₂ nanoflowers for photo- and humidity sensor applications. *Sens. Actuators A Phys.* **2019**, *295*, 160–168. [[CrossRef](#)]
30. Holzwarth, U.; Gibson, N. The Scherrer equation versus the ‘Debye-Scherrer equation’. *Nat. Nanotechnol.* **2011**, *6*, 534. [[CrossRef](#)]
31. Qiao, W.; Yu, L.; Chang, J.; Yang, F.; Feng, L. Efficient bi-functional catalysis of coupled MoSe₂ nanosheet/Pt nanoparticles for methanol-assisted water splitting. *Chin. J. Catal.* **2023**, *51*, 113–123.
32. Avsar, A.; Ciarrocchi, A.; Pizzochero, M.; Unuchek, D.; Yazyev, O.V.; Kis, A. Defect induced, layer-modulated magnetism in ultrathin metallic PtSe₂. *Nat. Nanotech.* **2019**, *14*, 674–678. [[CrossRef](#)] [[PubMed](#)]
33. Li, Z.; Liao, Y.; Liu, Y.; Zeng, W.; Zhou, Q. Room temperature detection of nitrogen dioxide gas sensor based on Pt-modified MoSe₂ nanoflowers: Experimental and theoretical analysis. *Appl. Surf. Sci.* **2023**, *610*, 155527. [[CrossRef](#)]
34. Dong, N.; Li, Y.; Feng, Y.; Zhang, S.; Zhang, X.; Chang, C.; Fan, J.; Zhang, L.; Wang, J. Optical limiting and theoretical modelling of layered transition metal dichalcogenide nanosheets. *Sci. Rep.* **2015**, *5*, 14646. [[CrossRef](#)] [[PubMed](#)]
35. Zhu, S.; Yang, C.; Li, F.; Li, T.; Zhang, M.; Cao, W. Improved photocatalytic Bi₂WO₆/BiOCl heterojunctions: One-step synthesis via an ionic-liquid assisted ultrasonic method and first-principles calculations. *Mol. Catal.* **2017**, *435*, 33–48.
36. Sidorowicz, A.; Yigit, N.; Wicht, T.; Stöger-Pollach, M.; Concas, A.; Orrù, R.; Cao, G.; Rupprechter, G. Microalgae-derived Co₃O₄ nanomaterials for catalytic CO oxidation. *RSC Adv.* **2024**, *14*, 4575–4586.

Disclaimer/Publisher’s Note: The statements, opinions and data contained in all publications are solely those of the individual author(s) and contributor(s) and not of MDPI and/or the editor(s). MDPI and/or the editor(s) disclaim responsibility for any injury to people or property resulting from any ideas, methods, instructions or products referred to in the content.